

## Supporting information

### Phenazine conjugated microporous polymer-based quartz crystal microbalance for sensitive detection of formaldehyde vapors at room temperature: an experiment and density functional theory study

Mohammed G. Kotp,<sup>a</sup> Nagy L. Torad,<sup>b,c,\*</sup> Johann Lüder,<sup>a,d</sup> Watcharop Chaikittisilp,<sup>b,e</sup> Yusuke Yamauchi<sup>b,f</sup> Ahmed F. M. EL-Mahdy<sup>a,g,\*</sup>

<sup>a</sup> *Department of Materials and Optoelectronic Science, National Sun Yat-Sen University, Kaohsiung, 80424, Taiwan*

<sup>b</sup> *JST-ERATO Yamauchi Materials Space-Tectonics Project and International Center for Materials Nanoarchitectonics (WPI-MANA), National Institute for Materials Science (NIMS), 1-1 Namiki, Tsukuba, Ibaraki 305-0044, Japan*

<sup>c</sup> *Chemistry Department, Faculty of Science, Tanta University, Tanta 31527, Egypt*

<sup>d</sup> *Center for Theoretical and Computational Physics, National Sun Yat-Sen University, Kaohsiung 80424, Taiwan*

<sup>e</sup> *Research and Services Division of Materials Data and Integrated System (MaDIS), National Institute for Materials Science (NIMS), 1-1 Namiki, Tsukuba, Ibaraki 305-0044, Japan*

<sup>f</sup> *Australian Institute for Bioengineering and Nanotechnology (AIBN) and School of Chemical Engineering, The University of Queensland, Brisbane, QLD 4072, Australia*

<sup>g</sup> *Chemistry Department, Faculty of Science, Assiut University, Assiut 71516, Egypt*

Corresponding Authors:

E-mail: [ahmedelmahdy@mail.nsysu.edu.tw](mailto:ahmedelmahdy@mail.nsysu.edu.tw) (A. F. M. EL-Mahdy).

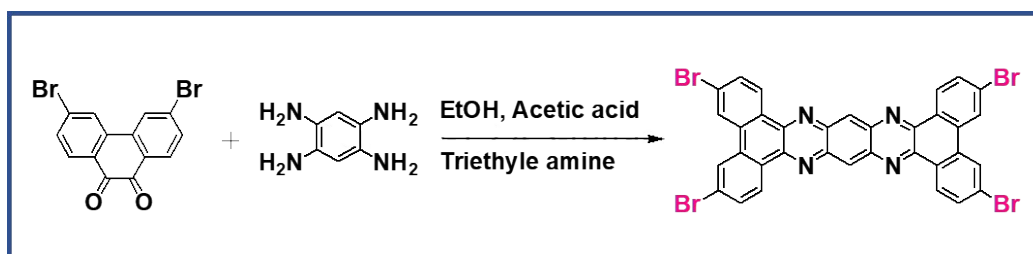
E-mail: [TORAD.Nagy@nims.go.jp](mailto:TORAD.Nagy@nims.go.jp) (N. L. Torad)

## 1. Materials

Starting chemicals, reagents and solvents are of analytical grades and were purchased from commercial providers. All chemicals were used for chemical reactions synthesis without any further purifications.

## 2. Synthetic procedures

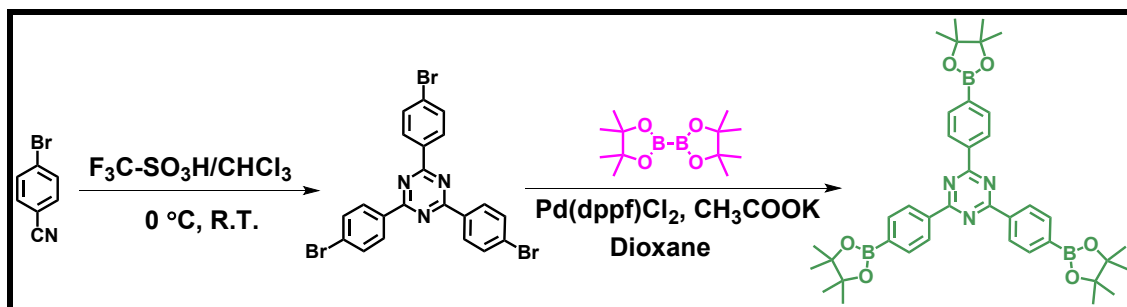
**2.1. 3,6,14,17-tetrabromodibenzo[a,c]dibenzo[5,6:7,8]quinoxalino[2,3-i]phenazine (QP-4Br):** According to recently reported method,<sup>S1</sup> the 3,6-dibromophenanthrene-9,10-dione (3,6-DBPD, 0.76 g, 2.1 mmol), 1,2,4,5-benzenetetramine tetrahydrochloride (TAB, 0.28 g, 1 mmol) were mixed in a mixture of ethanol (6 mL) and acetic acid (20 mL) under magnetic stirring and N<sub>2</sub> flow at 100 °C until to obtain a homogeneous mixture (Scheme S1). After that, triethylamine (1 mL) was injected into the feeding vessel and then the mixture was refluxed at 130 °C for 6 h. The obtained precipitate was filtered and thoroughly washed with methanol, acetone and THF. The product was then dried in a convection oven at 80 °C under vacuum for 12 h. FTIR profile shows the presence of characteristic bands at 1698, 1578, 1488 and 823 cm<sup>-1</sup> (Fig. S1).



**Scheme S1.** Synthesis of QP-4Br.

**2.2. 2,4,6-Tris(4-bromophenyl)-1,3,5-triazine (TPT-3Br):** According to our very recently published report,<sup>S2</sup> 4-bromobenzonitrile (1.5 g, 8.24 mmol) was dissolved in a dry CHCl<sub>3</sub> (20 mL), then was poured into a 100-mL two-neck round flask containing trifluoromethanesulfonic acid (4 mL, 0.045 mmol) under magnetic stirring in an ice bath for 30 min. After that, the reaction mixture was continuously stirred at ambient temperature for 24 h. The obtained product was extracted after pouring the suspension into an ice water, followed by neutralization with ammonium hydroxide. Finally, the solid precipitate was dried in a convection oven under vacuum at room temperature. FTIR measurements show the presence of characteristic bands at 1630 cm<sup>-1</sup>, 1582 cm<sup>-1</sup> and 1504 cm<sup>-1</sup>. <sup>1</sup>H NMR (CDCl<sub>3</sub>, 25 °C, 600 MHz): 8.60 (d, *J* = 12 Hz, 6H), 7.71 (d, *J* = 12Hz, 6H). <sup>13</sup>C NMR (CDCl<sub>3</sub>, 25 °C, 500 MHz): 171.10, 134.77, 132.01, 130.48 and 127.84 ppm.<sup>S2</sup>

**2.3. 2,4,6-tris(4-(4,5-dimethyl-1,3,2-dioxaborolan-2-yl)phenyl)-1,3,5-triazine (TPT-3Bpin):** To prepare TPT-3Bpin, the as-synthesized TPT-3Br was mixed with bis(pinacolato)diboron (0.85 g, 3.65 mmol), potassium acetate (0.3 g, 3.3 mmol), 1,1'-Bis(diphenylphosphino)ferrocene]dichloropalladium(II) (Pd(dppf)Cl<sub>2</sub>, 0.5 g, 0.7 mmol) and dissolved in 1,4-dioxane (50 mL), then the mixture was refluxed at 100 °C under N<sub>2</sub> gas for 24 h (Scheme S2). The reaction was left undisturbed to cool down at ambient temperature then poured into cold water containing ice cubes. Finally, the solid precipitate was extracted by dichloromethane, then was dried in a convection oven at 60 °C under vacuum. Furthermore, the obtained powder was finely purified using column chromatography (SiO<sub>2</sub>; THF/Hexane = 1:4). FTIR (Fig. S4); 2976 cm<sup>-1</sup>, 1700 cm<sup>-1</sup>, 1510 cm<sup>-1</sup> and 1341cm<sup>-1</sup>. <sup>1</sup>H NMR (CDCl<sub>3</sub>, 25 °C, 600 MHz) (Fig. S2); 8.62 ppm (d, 6H, *J* = 8.0 Hz), 7.90 ppm (d, 6H, *J* = 8.0 Hz) and 1.32 ppm (s, 36H). <sup>13</sup>C NMR (CDCl<sub>3</sub>, 25 °C, 125 MHz) (Fig. S6); 172.53, 139.34, 135.73, 128.67, 84.47 and 59.42 ppm.

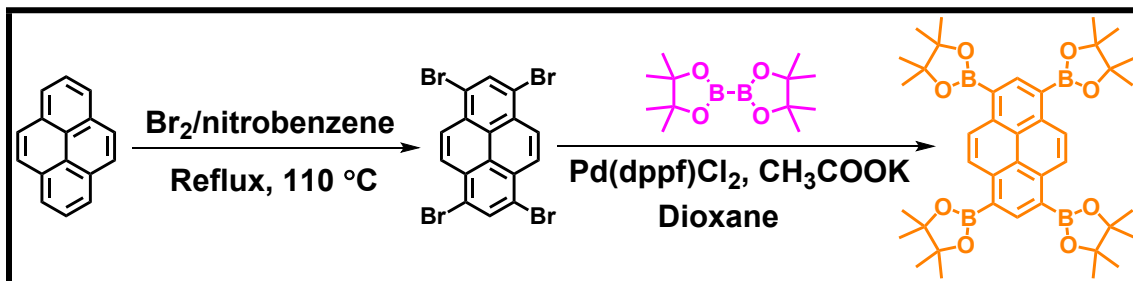


**Scheme S2.** Synthesis of TPT-3Bpin.

**2.4. 1,3,6,8-tetrabromopyrene (Pyrene-4Br):** According to our recent study,<sup>S3</sup> pyrene (5 g, 24 mmol) was mixed with nitrobenzene (200 mL), followed by a dropwise addition of bromine (5.6 mL, 109 mmol) to the reaction mixture. The mixture was then refluxed at 120 °C for 15 h. The obtained yellow solid crystals were filtered and thoroughly washed with ethanol for several times. Finally, the product was dried in an oven at 60 °C under vacuum for 12 h. Characteristic FTIR bands are appeared at 3078, 1587, 1450, 1228, 1052, 988, 862 and 812  $\text{cm}^{-1}$ .<sup>S3</sup>

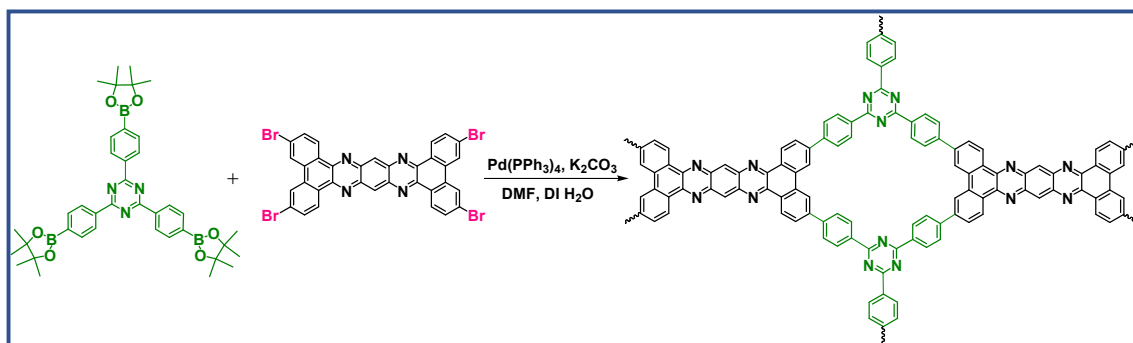
**2.5. 1,3,6,8-tetrakis(4,4,5,5-tetramethyl-1,3,2-dioxaborolan-2-yl)pyrene (Py-4Bpin):** To prepare Py-4Bpin, the as-synthesized Py-4Br (2 g, 3.8 mmol) was mixed with bis(pinacolato)diboron (5.98 g, 23.56 mmol), [1,1'-bis(diphenylphosphino)ferrocene]dichloro palladium(II) ( $\text{Pd}(\text{dppf})\text{Cl}_2$ , 241 mg, 0.033 mmol) and potassium acetate (2.33 g, 23.37 mmol) in a 100-mL two-neck round flask, then was degassed for 15 min (Scheme S3). After that, dioxane (40 mL) was injected, followed by refluxing at 100 °C under  $\text{N}_2$  gas for 48 h. The mixture was poured into cold water containing ice cubes, which immediately turned to yellow. The final product was filtered and washed by copious amount of water, then was finely purified with column chromatography using a suitable eluent of THF/hexane to remove the excess amount of catalyst and other impurities. The collected precipitate was recrystallized in methanol to obtain Py-4Bpin. After filtration, the product was dried in a convection oven at 60 °C under vacuum for 12 h. FTIR

bands (Fig. S5); 2964  $\text{cm}^{-1}$ , 1611  $\text{cm}^{-1}$ , 1555  $\text{cm}^{-1}$  and 1331  $\text{cm}^{-1}$ .  $^1\text{H}$  NMR ( $\text{CDCl}_3$ , 25  $^\circ\text{C}$ , 600 MHz) (Fig. S3); 9.1 ppm (s, 2H), 8.9 ppm (s, 4H), and 2.21 ppm (s, 48H).  $^{13}\text{C}$  NMR ( $\text{CDCl}_3$ , 25  $^\circ\text{C}$ , 125 MHz) (Fig. S6); 138.5, 129.85, 124.46, 84.18 and 25.76 ppm.



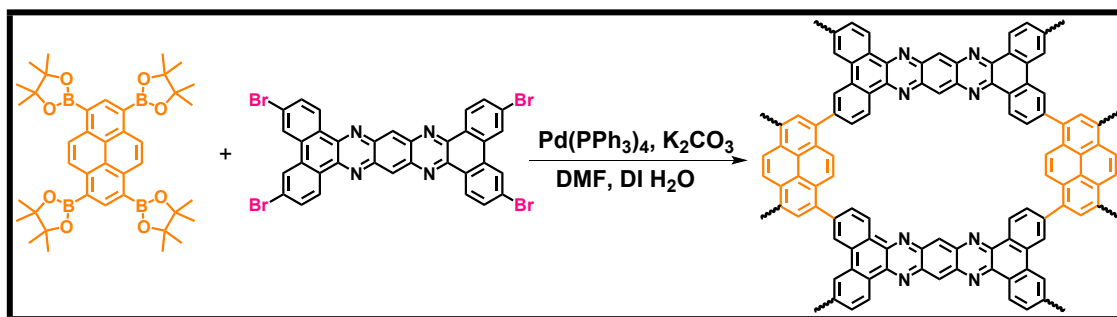
**Scheme S3.** Synthesis of Py-4Bpin.

**2.6. Synthesis of TPT-QP conjugated microporous polymer (CMP):** The as-synthesized monomers QP-4Br (150 mg, 0.18 mmol) and TPT-3Bpin (173 mg, 0.2 mmol) were mixed together with  $\text{Pd}(\text{PPh}_3)_4$  (50 mg, 0.04 mmol) and  $\text{K}_2\text{CO}_3$  (260 mg, 1.8 mmol) in an Schlenk tube, followed by degassing for 15 min (Scheme S4). A co-solvent of DMF (10.34 mL) and water (1.3 mL) was added to the reaction mixture. After that, the feeding tube was treated with a triple freeze-thaw cycle. The reaction was conducted under continuous stirring at 130  $^\circ\text{C}$  for 72 h. The resultant polymer was separated and thoroughly washed with methanol, hexane, acetone and THF using Soxhlet. Finally, the powder was then dried in a convection oven at 80  $^\circ\text{C}$  under vacuum. FTIR shows characteristic bands appeared at 3001, 1632, 1600 and 1512  $\text{cm}^{-1}$  (Fig. S4).



**Scheme S4.** Synthesis of TPT-QP CMP.

**2.7. Py-QP conjugated microporous polymer (CMP):** The synthesis process was followed as the one of TPT-QP CMP except Py-4Bpin was used instead (Scheme S5). The as-synthesized monomers Py-4Bpin (150 mg, 0.24 mmol), QP-4Br (170 mg, 0.21 mmol) were mixed with Pd(PPh<sub>3</sub>)<sub>4</sub> (40 mg, 0.03 mmol) and K<sub>2</sub>CO<sub>3</sub> (294 mg, 2.1 mmol) in Schlenk tube, followed by degassing for 15 min. A co-solvent of DMF (10 mL) and water (1.25 mL) was added, then the feeding tube was treated with a triple freeze-thaw cycle. After that, the reaction was conducted under continuous stirring at 130 °C for 72 h. The resultant polymer was centrifuged, then thoroughly washed with methanol, hexane, acetone and THF using Soxhlet. Finally, the powder was dried in a convection oven at 80 °C under vacuum. FTIR spectra shows characteristic bands at 3056, 1641, 1591 and 1510 cm<sup>-1</sup> (Fig. S5).



**Scheme S5.** Synthesis of Py-QP CMP.

### 3. Characterizations

Fourier-transform infrared spectrophotometer (FTIR, Bruker Tensor 27) was used to record FTIR spectra of the synthesized samples. INOVA 500 (INOVA 500MHz NMR) was used for recording <sup>1</sup>H and <sup>13</sup>C NMR portfolios through DMSO-*d*<sub>6</sub> and CDCl<sub>3</sub> as exterior solvents and chemical shifts were detected in parts per million (ppm). A Bruker Advance 400 NMR spectrometer and Bruker magic angle spinning (MAS) probe were employed for obtaining the solid state <sup>13</sup>C NMR (SSNMR) portfolios. <sup>13</sup>C NMR spectral data were acquired through cross-polarization with MAS (CPMAS)

at 75.5 MHz. Micromeritics ASAP 2020 surface area and porosity analyzer were employed for measuring N<sub>2</sub> adsorption-desorption isotherms of CMP samples. The Brunauer-Emmett-Teller (BET), *t*-plot, and the nonlocalized density functional theory (NLDFT) methods were used to analyze the specific surface area and pore structural properties of the obtained CMP materials, respectively. The surface areas of the polymer CMP materials were calculated based on the BET model by using the data of adsorption branches in the relative pressure ( $P/P_0$ ) range of 0.05-0.5. The morphological structure of the obtained CMP materials was identified by a field emission scanning electron microscope (FE-SEM, JEOL JSM-7610F) operated at an accelerating voltage of 5.0 kV and a transmission electron microscope (TEM, JEOL-2010 FEI Tecnai G20) equipped with field-emission microscope (JEOL, Tokyo, Japan) that was operated at high voltage of 200 kV. Thermogravimetric (TG) analysis was carried out using a TGA Q50 Thermogravimetric Analyzer in N<sub>2</sub> heating from room temperature to 800 °C at 20 °C·min<sup>-1</sup>. The chemical states and elemental compositions were evaluated from X-ray photoelectron spectroscopy (XPS) spectra using a British VG Scientific ESCALAB 250 system with an Al K $\alpha$  X-ray radiation source at 1486.6 eV. All the binding energies were calibrated *via* referencing to C1s binding energy (285.0 eV).

## Spectral Profiles of monomers and CMPs

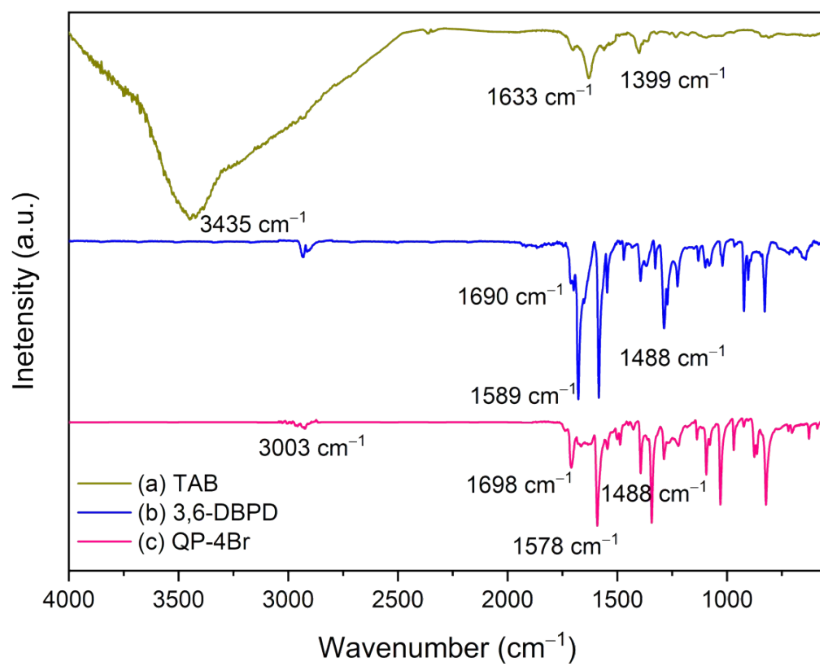


**Fig. S1.** FTIR spectra of (a) benzene-1,2,4,5-tetraamine tetrahydrochloride (TAB), (b) 3,6-dibromophenanthrene 9,10-dione (3,6-DBPD) and (c) QP-4Br.

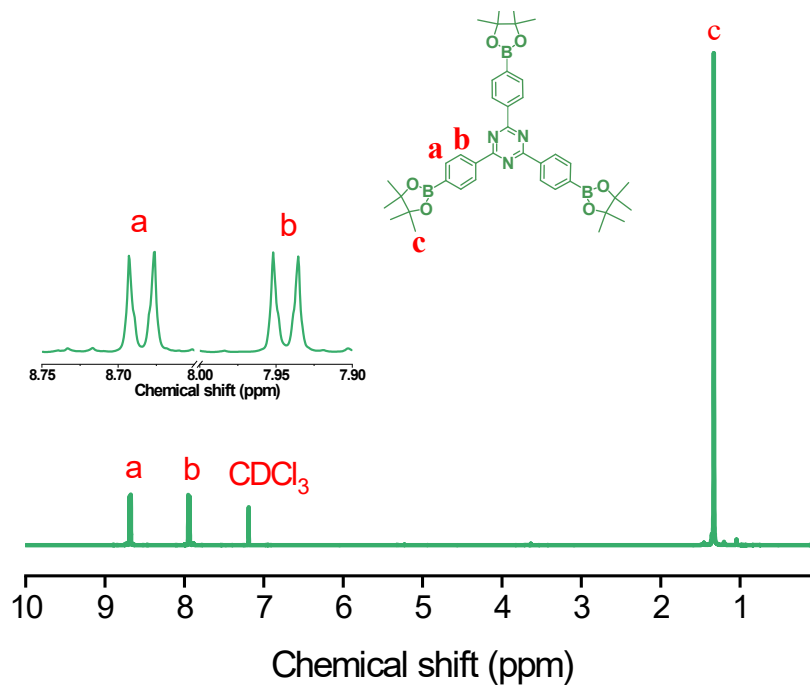


**Fig. S2.**  $^1\text{H}$  NMR spectrum of TPT-3Bpin.

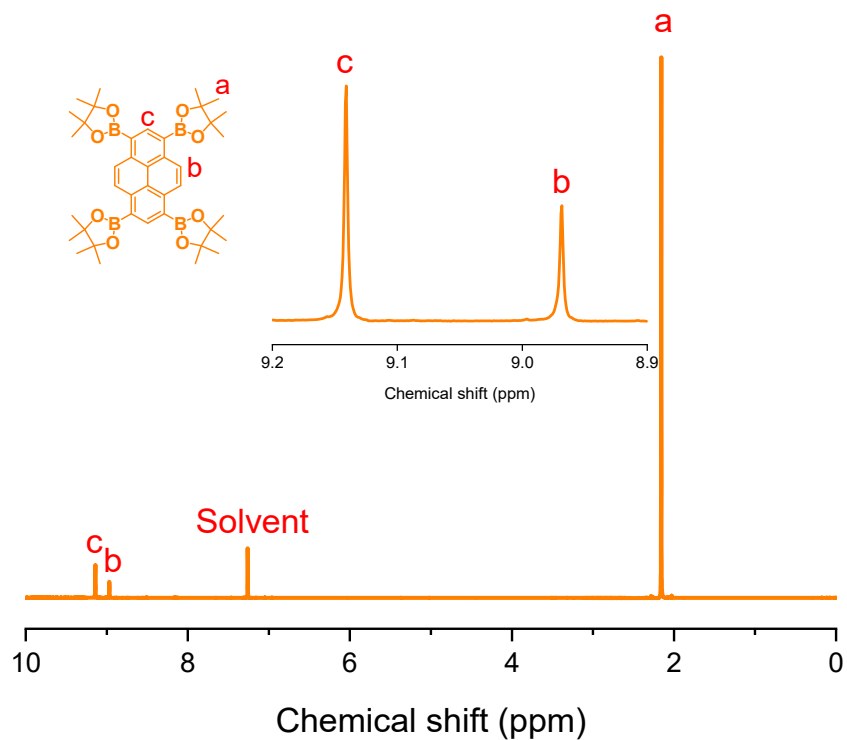


**Fig. S3.**  $^1\text{H}$  NMR spectrum of Py-4Bpin.

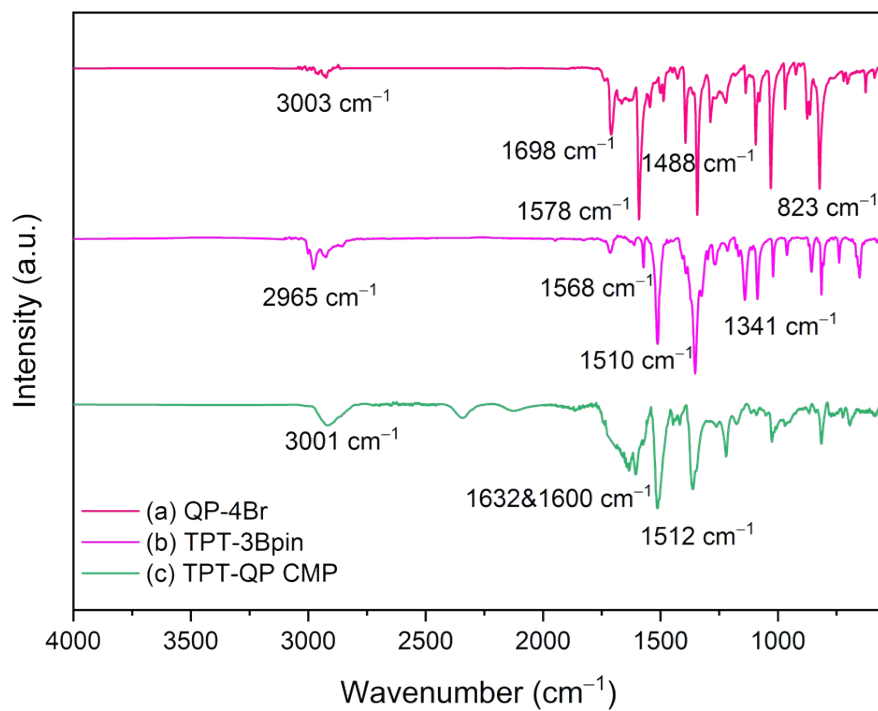


**Fig. S4.** FTIR spectra of (a) QP-4Br, (b) TPT-3Bpin and (c) TPT-QP CMP.

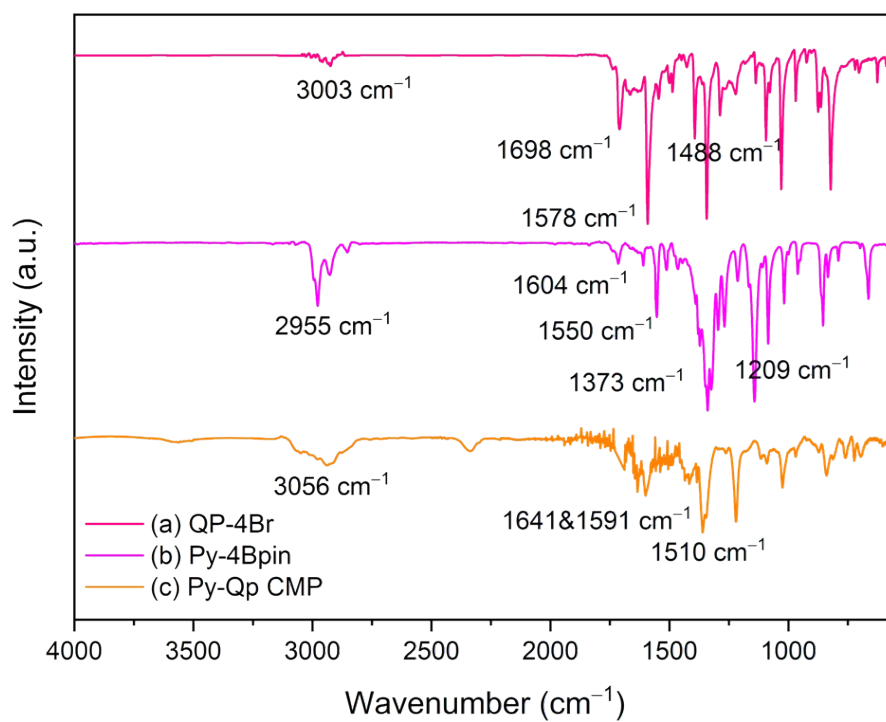


**Fig. S5.** FTIR spectra of (a) QP-4Br, (b) Py-4Bpin and (c) Py-QP CMP.

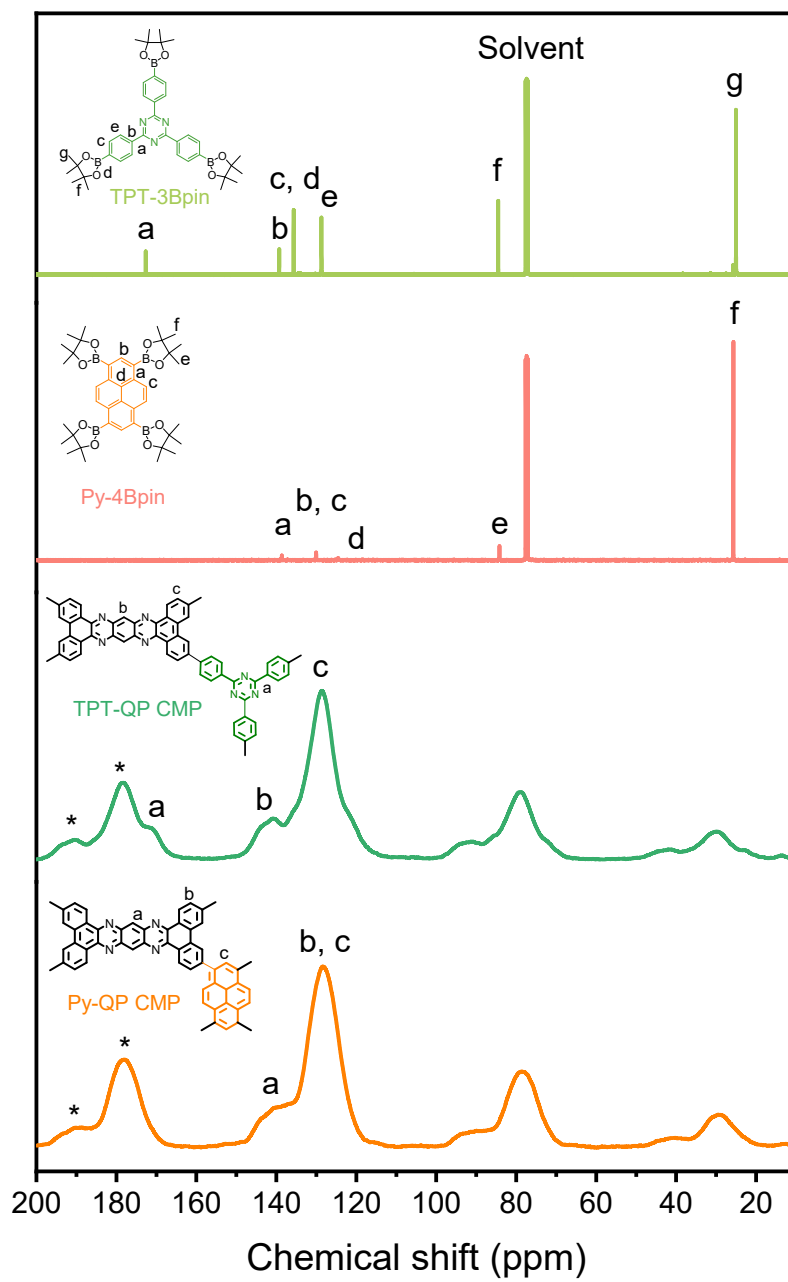


**Fig. S6.**  $^{13}\text{C}$  NMR profiles of TPT-3Bpin, Py-4Bpin and TPT-QP and Py-QP CMPs.

## XPS profile

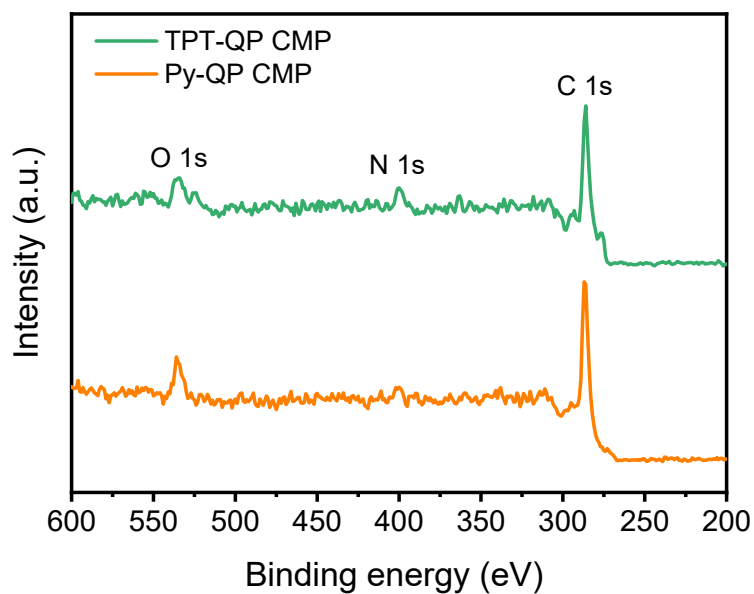


**Fig. S7.** High resolution wide-scan XPS profiles of TPT-QP and Py-QP CMPs.

## Thermogravimetric analysis

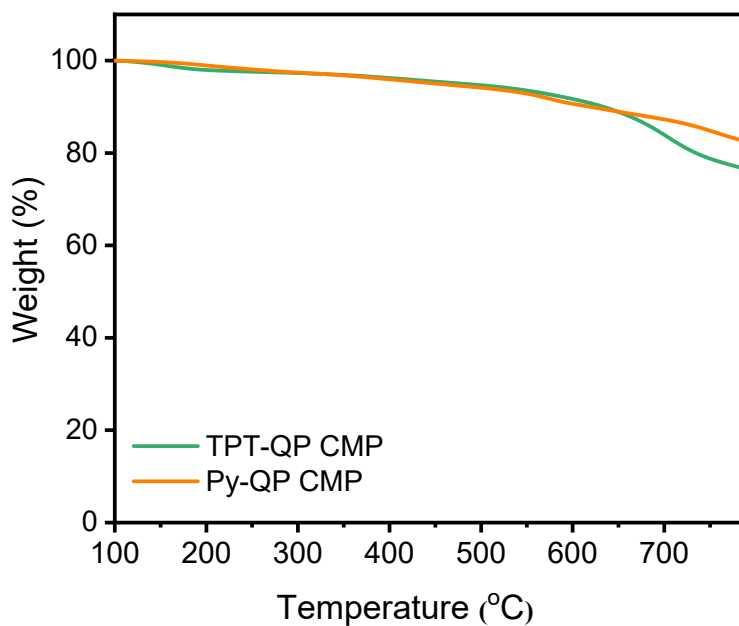


**Fig. S8.** Thermogravimetric analysis of (a) TPT-QP and (b) Py-QP CMPs under N<sub>2</sub> gas flow.

## TGA data and BET parameters

**Table S1.** Summary of textural and thermal properties of TPT-QP and Py-QP CMPs.

CMP	$S_{\text{BET}}$ ( $\text{m}^2 \text{g}^{-1}$ )	$V_{\text{total}}$ ( $\text{cm}^3 \text{g}^{-1}$ )	Pore size (nm)	Char yield (%)	$T_d$ ( $^{\circ}\text{C}$ )
TPT-QP	365.63	0.3335	0.63-1.66/3.45	76.5	591
Py-QP	527.22	0.3697	0.66-1.69/3.22	82.5	615

### 4. Quartz crystal microbalance gas sensor set up

For sensing HCHO vapors, the QCM sensor technique was used (AT-cut 9.0 MHz, model, QCA922, SEIKO EG&G Co. Ltd., Japan) to measure the frequency change caused by the adsorbed mass. Before coating the samples, the uncoated Au electrodes of the QCM sensor were soaked in an ethanol/water mixture (3:1) and sonicated for 30 min, then dried in an oven at 60 °C under vacuum. Their fundamental frequencies ( $F_0$ ) were recorded and these values of  $F_0$  were later used to estimate the masses of the CMPs samples coated onto the surface of the Au electrode using the Sauerbrey equation (Eq. (1)). To coat the electrodes, homogenous suspension solutions of CMPs samples (2 mg) were mixed with aqueous solutions of Nafion binder (1 mL/0.05 wt%) and then sonicated for 30 min. QCM electrodes were fabricated by drop-coating of the CMPs samples (5  $\mu\text{L}$ ) onto the surface of the Au-electrodes at ambient temperature, then they were left undisturbed for 30 min. After that, the electrodes were sequentially dried overnight in a convection oven under vacuum at 60 °C.

QCM sensor experiments were conducted by connecting TPT-QP or Py-QP CMPs-modified electrodes inside the testing vessel, and their frequencies were recorded after coating as  $F_1$  under a flow of  $\text{N}_2$  gas. A stable base lines ( $\pm 1 \text{ Hz min}^{-1}$ ) were observed, indicating good adherence of CMPs. All measurements were conducted under ambient conditions. Temperature and relative

humidity inside the glass vessel were measured at  $20 \pm 2$  °C and  $47 \pm 3\%$ , respectively. The gas-sensing properties of TPT-QP and Py-QP CMPs towards formaldehyde (HCHO) vapors were studied in the presence of other vaporized substances including ammonia (NH<sub>3</sub>), pyridine (C<sub>5</sub>H<sub>5</sub>N), ethanol (CH<sub>3</sub>CH<sub>2</sub>OH), chloroform (CHCl<sub>3</sub>), carbon tetrachloride (CCl<sub>4</sub>), benzene (C<sub>6</sub>H<sub>6</sub>), cyclohexane (*c*-C<sub>6</sub>H<sub>12</sub>) and 1,2-dichloroethane (1,2-CH<sub>2</sub>CH<sub>2</sub>Cl<sub>2</sub>) in the static sensing system by measuring the frequency change ( $\Delta F$ , Hz) of the QCM caused by vapor species additional mass at room temperature. The vapor analyte-saturated TPT-QP or Py-QP-modified QCM electrodes was treated with a flow of N<sub>2</sub> purged through the testing glass vessel to desorb the chemical analyte molecules until a baseline frequency response was obtained. The return of the electrode to its initial frequency was taken as an indication of full desorption of the chemical-vapor analyte. During sequential injection of the liquid analyte, the time-dependent frequency was automatically recorded on a PC running the WinQCM software measurement program.

The change in oscillation frequency caused by the additional adsorbed mass of chemical-vapor analyte can be precisely measured using the QCM sensor technique at the nanogram range. The relation between  $\Delta F$  (Hz) and the mass per unit area,  $\Delta m$  (g cm<sup>-2</sup>) deposited onto the Au electrode of the QCM sensor at a fundamental resonant frequency,  $F_0$ , was investigated by Sauerbrey as described in Eq. (S1).<sup>S4</sup>

$$\Delta F = -\frac{2NF_0^2\Delta m}{\sqrt{\rho\mu} A} \dots\dots\dots(S1)$$

$$\Delta F = F_1 - F_0 \dots\dots\dots(S2)$$

where N,  $F_0$ ,  $\rho$ ,  $\mu$ , and  $A$  express the harmonic overtone, fundamental resonance frequency of the crystal (Hz), density of quartz (2.649 g cm<sup>-3</sup>), elastic shear modulus ( $2.947 \times 10^{11}$  g cm<sup>-1</sup> s<sup>-2</sup>), and electrode surface area (5 mm diameter, 0.196 cm<sup>2</sup>), respectively. To estimate the mass of the sample deposited on the QCM electrode,  $\Delta F$  was recorded after drop-coating of the TPT-QP and Py-QP

CMP samples as 7,871.4 and 8,120.2 Hz, thus the mass of the TPT-QP and Py-QP deposited on the Au surface of the electrode was 2.48 and 2.56  $\mu\text{g}$ , respectively. All the recorded frequencies were normalized by mass to determine the sensor sensitivity and selectivity.

Small volumes of the liquid analytes vaporized rapidly after injection inside the 1.55-L testing glass vessel and the gaseous chemical-analytes were obtained at ambient temperature ( $22 \pm 2$  °C) by injecting an appropriate volume of the liquid analyte using a Hamilton microliter syringe (Hamilton Company Inc., Switzerland) and the vapor concentration was calculated in ppm based on its density and mass concentration according to the following formula (Eq. (S3)):<sup>S4</sup>

$$C_{ppm} = \frac{22.4\rho TV_s}{273MV} \times 10^3 \dots\dots\dots(S3)$$

where  $C_{ppm}$  refers to the analyte concentration (ppm),  $\rho$  is the density of injected liquid analyte ( $\text{g mL}^{-1}$ ),  $T$  is the working temperature (K),  $M$  is the molecular weight of injected chemical-analyte (g), and  $V_s$  and  $V$  represent the volumes of the injected chemical-analyte ( $\mu\text{L}$ ) and the working glass vessel volume (L), respectively.

The structural properties of CMP materials can influence the adsorption rate of HCHO vapor, which is controlled by the surface area, porosity and morphology. Therefore, the adsorption of HCHO molecules can be considered as a pseudo-first-order mass transfer between the vapor phase and the CMP material, which can be investigated by real-time monitoring of the frequency immediately after injection of HCHO into the glass vessel. Pseudo first-order kinetic model was applied to fit the experimental  $\Delta F_t$ s of the QCM sensor. The pseudo first-order kinetic rate constant ( $k_1$ ), which expresses the initial rate of uptake of HCHO vapors ( $\Delta F_t/\Delta F_\infty$ ) was calculated using Eqs. (S4-6).<sup>S4</sup>

$$\frac{\Delta F_t}{\Delta F_\infty} = 1 - e^{-k_1 t} \dots\dots\dots(S4)$$

$$\ln\left(1 - \frac{\Delta F_t}{\Delta F_\infty}\right) = -k_1 t \dots\dots\dots(S5)$$

$$\Delta F_t = F - F_t \text{ and } \Delta F_\infty = F - F_\infty \dots(S6)$$

where  $\Delta F_t$  and  $\Delta F_\infty$  refer to the frequency changes for vapor uptake at time ( $t$ ) and at equilibrium, respectively.  $k_1$  ( $\text{min}^{-1}$ ) is the adsorption rate constant of pseudo-first order kinetic model.  $F$  is the oscillating crystal frequency before exposure to the analyte at  $t = 0$ , and  $F_t$  and  $F_\infty$  are the crystal frequency after injection of analyte at time ( $t$ ) and at equilibrium, respectively.

**Table S2.** Summary of hazardous formaldehyde vapor sensing performances of various

<b>Sensing substrate</b>	<b>Surface area (m<sup>2</sup> g<sup>-1</sup>)</b>	<b>Coating technique</b>	<b>Sensitivity (Hz ppm<sup>-1</sup>)</b>	<b>LOD (ppm)</b>	<b>Reference</b>
<b>Carbon quantum dots (CQDs)</b>	NA	Drop-casting method	42.61	2.9	S5
<b>Polyethyleneimine (PEI)/poly(vinyl alcohol) (PEI/PVA)</b>	NA	Electrospinning-deposition	0.5	10	S6
<b>Polyethyleneimine (PEI) modified@fibrous PS (PEI-PS)</b>	11.67	Electrospinning	1.7	3	S7
<b>Chitosan-PEI nanocomposite</b>	8.25	Electrospinning/netting	NA	5	S8
<b>Graphene oxide</b>	NA	Drop-casting method	22.9	0.06	S9
<b>Polyaniline-TiO<sub>2</sub> nanocomposite</b>	NA	Dispensing	NA	150	S10
<b>Zeolitic imidazolate framework (ZIF), ZIF-67</b>	NA	Paste-casting	NA	5.0	S11
<b>ZIF-8/MWCNT nanocomposite</b>	1412.76	Drop-casting method	NA	4.83	S12
<b>TPT-QP CMP</b>	527	Drop-casting method	2.4	2.6	This work

## 5. Computational Setup

In the assessment of atomistic insight into the sorption mechanism, we performed Density Functional Theory (DFT) calculations. The interaction strength between molecular units of TPT-QP or Py-QP CMPs with HCHO were computed with the Gaussian software package.<sup>S13</sup> The B3LYP hybrid functional with additional Grimme-D3 dispersion corrections<sup>S14</sup> to accurately account for van der Waals interactions ensured accurate calculations of adsorption energies between molecules. The electronic wave functions were represented with LanL2DZ basis set which allows efficient computations for large systems sizes. The adsorption energies were computed as described in Eq. (S7):

$$E_{ads} = E_{CMP+HCHO} - E_{HCHO} - E_{CMP} \quad (S7)$$

where the first term on the right-hand side ( $E_{CMP+HCHO}$ ) equals to the total energy of the optimized complex formed by CMP with one HCHO adsorbent, while the second ( $E_{HCHO}$ ) and third terms ( $E_{CMP}$ ) refer to the total energy of the optimized individual HCHO and CMP, respectively. To find the molecular arrangements with the strongest binding strength, several initial adsorption sites at the CMP and orientations of the HCHO were probed. In addition, we perform a multivariant linear regression of  $\Delta F$  to simple molecular properties of the gases in this study including their polarizability ( $P$ ), permanent dipole moment ( $D$ ), and van der Waals coefficients  $a$  and  $b$  known from the van der Waal's equation of state for a non-ideal gas. In addition, a contribution of induced dipole is considered by a quadratic term in  $D$ . Then, we assume and compare predict and measured values of  $\Delta F$  based on Eq. (S8).

$$\Delta F \propto c_0 + c_1P + c_2D + c_3a + c_4b + c_5D^2 \quad (S8)$$

Through the results from DFT simulations in combination with this simple model, and selection of certain terms within the model, we can estimate the importance of some of the molecular properties and their role in the selectivity of the CMPs and provide a semi-empirical

explanation.

**Table S3.** Results of the multivariant regression model.

	P+D+vdW [-D <sup>2</sup> ]		vdW [-D <sup>2</sup> ]		P+D[-D <sup>2</sup> ]	
	TPTQP	PyQP	TPTQP	PyQP	TPTQP	PyQP
$c_0/Hz/\mu g$	0	0	0	0	0	0
$c_1/\text{\AA}^3$	-17.3 [-38.1]	-35.3 [-40.4]	0	0	9.07	-0.475
$c_2/Debye$	128.8 [-65.72]	41.7 [-6.13]	0	0	-29.38	6.75
$\frac{L^2 bar}{c_3/mol^2}$	38.4 [65.97]	15.3 [22.13]	39.84 [22.03]	-2.78 [-1.40]	0	0
$\frac{L}{c_4/mol}$	-4646 [-8531]	327.7 [-627.6]	-6735 [-3078]	640.6 [356.0]	0	0
$c_5/Debye^2$	-80 [0.0]	-19.7 [0.0]	-26.48 [0]	2.06 [0]	0	0
$R^2$	0.904 [0.393]	0.895 [0.742]	0.574 [-1.565]	-32.0 [-19.09]	-1.06	-19.1

## References

- S1 W. Liu, M. Ulaganathan, I. Abdelwahab, X. Luo, Z. Chen, S. J. R. Tan, X. Wang, Y. Liu, D. Geng, Y. Bao, J. Chen and K. P. Loh, *ACS nano*, 2018, **12**, 852-860.
- S2 A. M. Elewa, A. F. M. El-Mahdy, M. H. Elsayed, M. G. Mohamed, S.-W. Kuo and H.-H. Chou, *Chem. Eng. J.*, 2021, **421**, 129825.
- S3 M. G. Kotp, A. M. Elewa, A. F. M. El-Mahdy, H.-H. Chou and S.-W. Kuo, *ACS Appl. Energy Mater.*, 2021, **4**, 13140-13151.
- S4 N. L. Torad, H. El-Hosainy, M. Esmat, K. E. El-Kelany, R. Tahawy, J. Na, Y. Ide, N. Fukata, W. Chaikittisilp, J. P. Hill, X. Zhang, M. El-Kemary and Y. Yamauchi, *ACS Appl. Mater. Interfaces*, 2021, **13**, 48595-48610.
- S5 W. A. Amer, A. F. Rehab, M. E. Abdelghafar, N. L. Torad, A. S. Atlam and M. M. Ayad, *Carbon*, 2021, **179**, 159-171.
- S6 X. Wang, B. Ding, M. Sun, J. Yu and G. Sun, *Sens. Actuators B Chem.*, 2010, **144**, 11-17.
- S7 C. Zhang, X. Wang, J. Lin, B. Ding, J. Yu and N. Pan, *Sens. Actuators B Chem.*, 2011, **152**, 316-323.
- S8 N. Wang, X. Wang, Y. Jia, X. Li, J. Yu and B. Ding, *Carbohydr. Polym.*, 2014, **108**, 192-199.
- S9 M. Yang and J. He, *Sens. Actuators B Chem.*, 2016, **228**, 486-490.
- S10 J. Zheng, G. Li, X. Ma, Y. Wang, G. Wu and Y. Cheng, *Sens. Actuators B Chem.*, 2008, **133**, 374-380.
- S11 E.-X. Chen, H. Yang and J. Zhang, *Inorg. Chem.*, 2014, **53**, 5411-5413.
- S12 N. Jafari and S. Zeinali, *ACS Omega*, 2020, **9**, 4395-4402.
- S13 M. Frisch, G. Trucks, H. Schlegel, G. Scuseria, M. Robb, J. Cheeseman, G. Scalmani, V. Barone, G. Petersson and H. Nakatsuji. Gaussian 16. Gaussian, Inc. Wallingford, CT 2016.
- S14 J. Moellmann and S. Grimme, *J. Phys. Chem. C*, 2014, **118**, 7615-7621.